Single nanowire spectrometers

Authors: Zongyin Yang[1†], Tom Albrow-Owen[1†], Hanxiao Cui[2], Jack Alexander-Webber[2], Fuxing Gu[3], Xiaomu Wang[4], Tien-Chun Wu[1], Minghua Zhuge[5], Calum Williams[2], Pan Wang[6], Anatoly V. Zayats[6], Weiwei Cai[7], Lun Dai[8], Stephan Hofmann[2], Mauro Overend[2], Limin Tong[5], Qing Yang[5], Zhipei Sun[9,10], Tawfique Hasan[1*]

Affiliations:

[1]Cambridge Graphene Centre, University of Cambridge, Cambridge, CB3 0FA, UK.

[2]Department of Engineering, University of Cambridge, Cambridge CB3 0FA, UK.

[3]Shanghai Key Laboratory of Modern Optical System, University of Shanghai for Science and Technology, Shanghai 200093, China.

[4]School of Electronic Science and Engineering, Nanjing University, Nanjing 210023, China.

[5]State Key Laboratory of Modern Optical Instrumentation, College of Optical Science and Engineering, Zhejiang University, Hangzhou 310027, China.

[6]Department of Physics and London Centre for Nanotechnology, King's College London, London, WC2R 2LS, UK.

[7]Key Lab of Education Ministry for Power Machinery and Engineering, School of Mechanical Engineering, Shanghai Jiao Tong University, Shanghai 200240, China.

[8]State Key Laboratory for Artificial Microstructure & Mesoscopic Physics, School of Physics, Peking University, Beijing 100871, China.

[9]Department of Electronics and Nanoengineering, Aalto University, Tietotie 3, FI-00076 Espoo, Finland.

[10]QTF Centre of Excellence, Department of Applied Physics, Aalto University, FI-00076, Espoo, Finland.

*Correspondence to: th270@cam.ac.uk

†These authors contributed equally to this work

Abstract:

Spectrometers with ever-smaller footprints are sought after for a wide range of applications where minimized size and weight is paramount, including emerging in-situ characterization techniques. We report on an ultra-compact micro-spectrometer design based on a single compositionally engineered nanowire. This platform is independent of the complex optical components or cavities that tend to constrain further miniaturization of current systems. We show that incident spectra can be computationally reconstructed from the different spectral response functions and measured photocurrents along the length of the nanowire. Our devices are capable of accurate, visible-range monochromatic and broadband light reconstruction, as well as spectral imaging from centimeter-scale focal planes down to lensless, single-cell-scale in-situ mapping.

One Sentence Summary: *An ultra-compact spectrometer based on a single, compositionally-engineered nanostructure is demonstrated*

Main Text:

Optical spectroscopy is one of the most ubiquitous, versatile characterization techniques across industrial processes and fundamental scientific research (*1*). A variety of miniaturized, portable spectrometers have been developed for applications where reduced footprint and weight takes precedence over high resolution (*2*). These micro-spectrometers have typically been inspired by conventional bench-top spectrometers, centering around interferometers or gratings, with miniaturized or integrated optics (*3-5*). When minimizing physical dimensions towards sub-millimeter scales desired in, for example, lab-on-a-chip systems, such designs are inherently limited by adverse effects associated with scaling their optical components or path lengths. Micro-spectrometers that use computational spectral reconstruction circumvent these constraints by addressing a full range of spectral components simultaneously at multiple detectors (*6, 7*). However, they have thus far been based on complex millimeter-scale arrays of individually prepared filters arranged over CCD or CMOS detectors, which are challenging to miniaturize.

Here, we demonstrate that a single compositionally-engineered nanowire can form the basis of an ultra-compact computational micro-spectrometer design, where the previously distinct elements which separate and detect light have been combined into an individual, micrometer-scale component grown in a single bottom-up process. These semiconductor nanowires are alloyed such that the composition, and thus the spectral response, varies along their length, given that photon absorption can only occur at energies above the bandgap of the respective nanowire segment (*8-11*). By electronically probing the photocurrent and cross-referencing with a pre-calibrated response function for each of a series of points along the nanowire, it is possible to computationally reconstruct incident light signals. With a sufficient number of points, and through careful optimization of the measurement stability, along with the development of a bespoke algorithm,

both monochromatic and broadband spectra can be accurately reconstructed. In this way, the entire active element of the spectrometer is scaled down to a footprint of just hundreds of nanometers in width and tens of micrometers in length, in a system that functions without the need for any complex or dispersive optics. The incorporation of our design into a mapping system allows spectral imaging from centimeter-scale image planes down to lensless, single-cell scale in-situ measurements.

Whilst epitaxial growth of thin-films with wide spatial compositional gradients is fundamentally difficult due to lattice mismatch with the substrate, the nanowire growth interface is independent of the substrate once nucleated (*12*). As such, nanowires can afford an almost arbitrary number of material systems to be alloyed into the same nanostructure through adjusting source vapors during growth (*13, 14*). This makes our spectrometer design highly versatile; the growth of nanowires with different composition-engineering straightforwardly realizes systems that could operate across any wavelength range from the infrared to ultraviolet (*11, 15, 16*).

The active element in our spectrometer is a compositionally-graded semiconducting CdS_xSe_{1-x} nanowire (*17, 18*), in which one end is composed mainly of elements Cd and S, and the other mainly of Cd and Se [(*19*), section MM1]. This corresponds to a continuous gradient of bandgaps spanning from 1.74 to 2.42 eV along their length (Fig. 1A). After transfer to a Si/SiO_2 substrate, electron-beam lithography is used to fabricate an array of parallel In/Au electrodes on the nanowire (Fig. 1B) [(*19*), section MM2]. To achieve stable electrical contacts, the nanowires are treated under nitrogen plasma, followed by immersion in ammonium sulfide solution immediately prior to metallization. The device is then encapsulated in Al_2O_3 via atomic layer deposition, to further enhance measurement stability [(*19*), section ST1]. Typical photodetector units, defined as between two neighboring electrodes, exhibit photoresponsivities of up to $\sim 1.4 \times 10^4$ AW^{-1} (Fig.

1C and Fig. S10) with a fast response and recovery time (~1.5 and ~3.5 ms, respectively, Fig. 1D). After fabrication, the spectrometer is calibrated by measuring the photocurrent as a function of wavelength for each of the *n* units [(*19*), section MM3]; these spectral response functions, $R_i(\lambda)$, where (i = 1, 2, … n), exhibit cutoff wavelengths that vary along the length of the nanowire (Fig. 1E).

During operation of the spectrometer (Fig. 1F) incident light represented by an unknown function, $F(\lambda)$, illuminates the device. Due to the small physical dimensions of the nanowire, we consider that the flux is spatially uniform across the device (Fig. S6). A data selector scans the photocurrent generated between each electrode pair, followed by signal processing. The measured photocurrent data, together with the pre-calibrated response functions are then processed (Figs. 1G-J) to reconstruct $F(\lambda)$ by solving a system of linear equations:

$$\int_{\lambda 1}^{\lambda 2} F(\lambda) R_i(\lambda)\, d\lambda = I_i \qquad (i = 1,2,3 \ldots, n) \tag{1}$$

where λ_1 and λ_2 define the spectrometer's operational wavelength range. Note that the reconstruction is only possible for incident light wavelengths within this range. The photocurrent I_i is the integral of $F(\lambda)R_i(\lambda)$ over the wavelength range (Fig. 1G, right-hand panels). For a spectrometer with *n* photodetector units, there are *n* sets of equations. Solving these equations by ordinary non-iterative methods is liable to breakdown because measurement errors in both $R_i(\lambda)$ and I_i make the equations ill-posed (*6, 20, 21*). In this case, the reconstructed target spectrum is fully distorted at the existing system noise level (Fig. S11). Further to minimizing measurement instabilities through optimizing fabrication, we introduce an adaptive Tikhonov regularization scheme to reduce the influence of these errors during the reconstruction [(*19*), section MM4 and Fig. S12]. The algorithm uses a linear combination of Gaussian basis functions with different amplitudes to fit the target spectrum (Fig. 1J).

We demonstrate the capability to reconstruct varied incident light spectra using two different nanowire spectrometers containing 30 and 38 photodetector units (Fig. 2). In resolving monochromatic light (Fig. 2A), the minimum reconstructed FWHM is equivalent to the optimal bandwidth of basis functions, which are ~8.5 nm and 7 nm for the 30-unit and 38-unit spectrometer, respectively. The spectrometers can resolve two peaks around 570 nm separated by 15 nm (Fig. 2B); peaks become indistinguishable once the separation is decreased to 10 nm (Fig. S13). Despite a reduction in footprint of ~2-3 orders of magnitude, such resolution is comparable to that of other visible-range spectral reconstruction microspectrometers, and commercially-available centimeter-scale systems (Table S1). Continuous broadband spectra can also be measured and reconstructed (Fig. 2C).

A number of routes exist to improve the resolution and reconstruction accuracy [(*19*), section ST2], through either collecting a greater quantity of measured data ($R_i(\lambda)$ and I_i), or reducing the prevalence and impact of measurement errors. The former can be achieved by increasing n, as demonstrated through comparison of the 30- and 38-unit devices (Figs. 2A, B) as well as device simulations (Fig. S14), or by increasing the sampling resolution in $R_i(\lambda)$. Addressing the latter, photocurrent magnitude and stability could be enhanced through further optimization of the nanowire growth or device fabrication and passivation. Additionally, at the calibration stage a light source with a narrower linewidth would reduce errors arising in $R_i(\lambda)$, whilst advancing the algorithm could enable more intelligent dampening of errors during the reconstruction process.

Monochromatic reconstruction performance remains consistent across the spectrometer's 130 nm bandwidth (Fig. 2D). Note that the spectral range is primarily limited by the material composition used in our nanowires. This could be readily increased by choosing other material compositions such as $Zn_xCd_{1-x}S_ySe_{1-y}$ (1.74-3.54 eV) (*15*), $In_xGa_{1-x}N$ (0.7-3.43 eV) (*16*) and Si_{1-}

$_xGe_x$ (0.66-1.12 eV) (*11*), enabling devices with spectral responses spanning from UV to infrared. Furthermore, in defining a bespoke set of spectral responses for each spectrometer, the calibration procedure acts to negate uncontrolled nanowire growth defects or minor fabrication variations between devices. This presents a significant advantage in the device manufacturability, taken alongside the scalability of all fabrication processes involved [(*19*), section ST4]. Correspondingly, reconstruction accuracy is reproducible across two devices with the same unit number (Fig. S15). Additionally, potential failure of individual units can be recognized and mitigated by the algorithm with minimal loss of reconstruction accuracy (Fig. S16). Performance of the spectrometers remains stable over two months, maintaining peak positional accuracy within 1 nm without recalibration (Fig. S17).

In many fields, such as astronomy (*22*), precision agriculture (*23*) and nanophotonics (*24*), spectral imaging [(*19*), section ST3] is in high demand to cross-analyze spectral and spatial information. We demonstrate spectral imaging using our 38-unit nanowire spectrometer *via* a spatial point-scanning strategy. An image is focused by a lens onto the device, which is then scanned across the focal plane on centimeter scales (Fig. 3A). In this scheme, the resolution is defined by the mapping step used, which can be equal to or larger than the device footprint; here we use a step of 0.3 mm. Photocurrents measured at each mapping step are recorded in a 3D (x, y, I_i) data cube (Fig. 3B). This initial cube is then converted to a spectral data cube (x, y, λ) by the reconstruction algorithm (Fig. 3C). Cross sections of this cube in the x-y plane are equivalent to single-wavelength spatial mapping (Fig. 3D). Applying standardized (International Commission on Illumination) color matching functions to the spectral cube produces a pseudo-colored image which is consistent with the original photograph (Fig. 3E). In addition, the reconstructed spectra are in good agreement with conventional spectrometer measurements of the same points (Fig. 3F).

Furthermore, we demonstrate in-situ, micrometer-scale spectral imaging using our nanowire spectrometer, which has long been a great challenge across fields such as cytobiology and biomedicine (*25, 26*). Given the typical footprint of the spectrometers is between 50-100 μm, the scanning method above must be adapted to achieve these resolutions. We adopt a shift register strategy, which sequences the measured photocurrent data with the measurement location for each unit (Fig. 4A). The spectral image data cube is reconstructed from the overlapping register region of the initial photocurrent data cube (Fig. 4B). The scanning step can be any integer multiple of the electrode array's pitch, meaning the maximum resolution is limited by the width of one unit (~1 μm for current devices).

A red onion cell membrane, featuring naturally colored cells surrounded by transparent cells, is mounted onto the holder and positioned over the nanowire spectrometer with a gap of several μm (Fig. 4C, D). During imaging, the nanowire spectrometer scans across the x-y plane beneath the membrane surface, under illumination by white light through the aperture, with a fixed mapping step (Fig. 4E). In this case, a step size of 10 units is chosen to shorten imaging time and avoid the cell membrane drying out during the measurement. Constrained by our stage setup, imaging time is currently limited by the movement and adjustment between points. More sophisticated scanning or imaging technologies [(*19*), section ST3] would allow higher resolution scans within the same timeframe. High-speed measurement could also be achieved through the development of a snapshot spectral imaging system based on a 2-dimensional spectrometer array. The intensity maps at fixed wavelengths and reconstructed absorption spectra for different points on the onion cells (Figs. 4F, G) illustrate the potential of these spectrometers to obtain spectral images at the cellular level.

The use of single compositionally-engineered nanowires enables an entire spectroscopy system to be miniaturized down to a scale of tens of micrometers, which could open new opportunities for almost any miniaturized spectroscopic application, including lab-on-a-chip systems, drones, implants, and wearable devices. Our proof of concept demonstrates a simple, versatile platform that can be expanded upon through a number of avenues by altering either the hardware or software of the system. Our study offers a practical step forward for other light sensitive nanomaterials to be directly exploited for customized design of ultra-miniaturized spectroscopy systems.

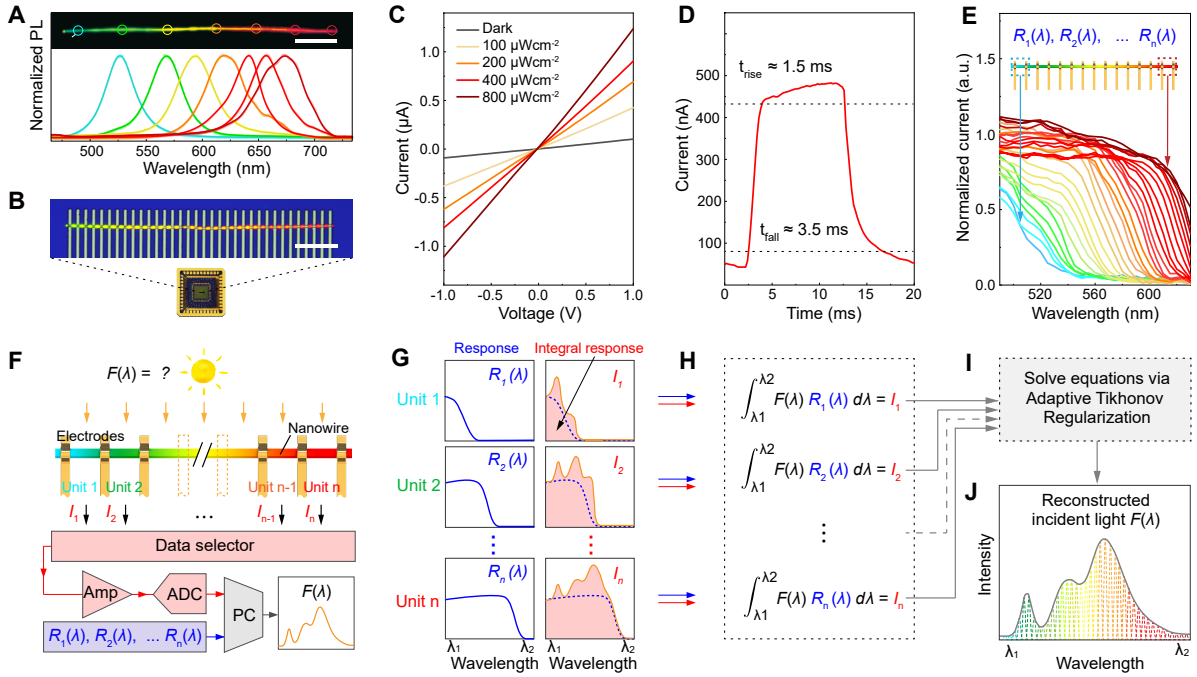

Fig. 1. Nanowire spectrometer design. (A) Real-color photoluminescence (PL) image of a typical compositionally-graded CdS_xSe_{1-x} nanowire and corresponding spectra collected from marked representative regions (spot size ~5 μm). Scale bar: 20 μm. **(B)** Fluorescent micrograph (top) of a typical nanowire spectrometer, incorporated into a packaged chip. Scale bar:10 μm. **(C)** I-V curves measured between two typical neighboring electrodes at the red (CdSe) end of the nanowire, illuminated with different intensities of 490 nm light. **(D)** Time response of the same photodetector unit under pulsed incident light (490 nm, 0.3 $mWcm^{-2}$) under 0.5 V bias. Dotted lines indicate 10 % and 90 % of peak value, as used for calculating the rise (1.5 ms) and fall time (3.5 ms). **(E)** Normalized spectral responses $R_i(\lambda)$ of each constituent unit in a typical spectrometer, with cut-off wavelengths varying continuously along the nanowire. **(F)** Operational schematic of the nanowire spectrometer. **(G)** Simulated spectral response $R_i(\lambda)$ and photocurrent I_i. Photocurrent is equal to the red area which indicates the integral responses to the incident light. **(H)** Mathematical description of the relation between $F(\lambda)$, $R_i(\lambda)$ and I_i. **(I)** Spectral reconstruction via solving the equation set. **(J)** Reconstructed spectrum of the simulated incident light $F(\lambda)$.

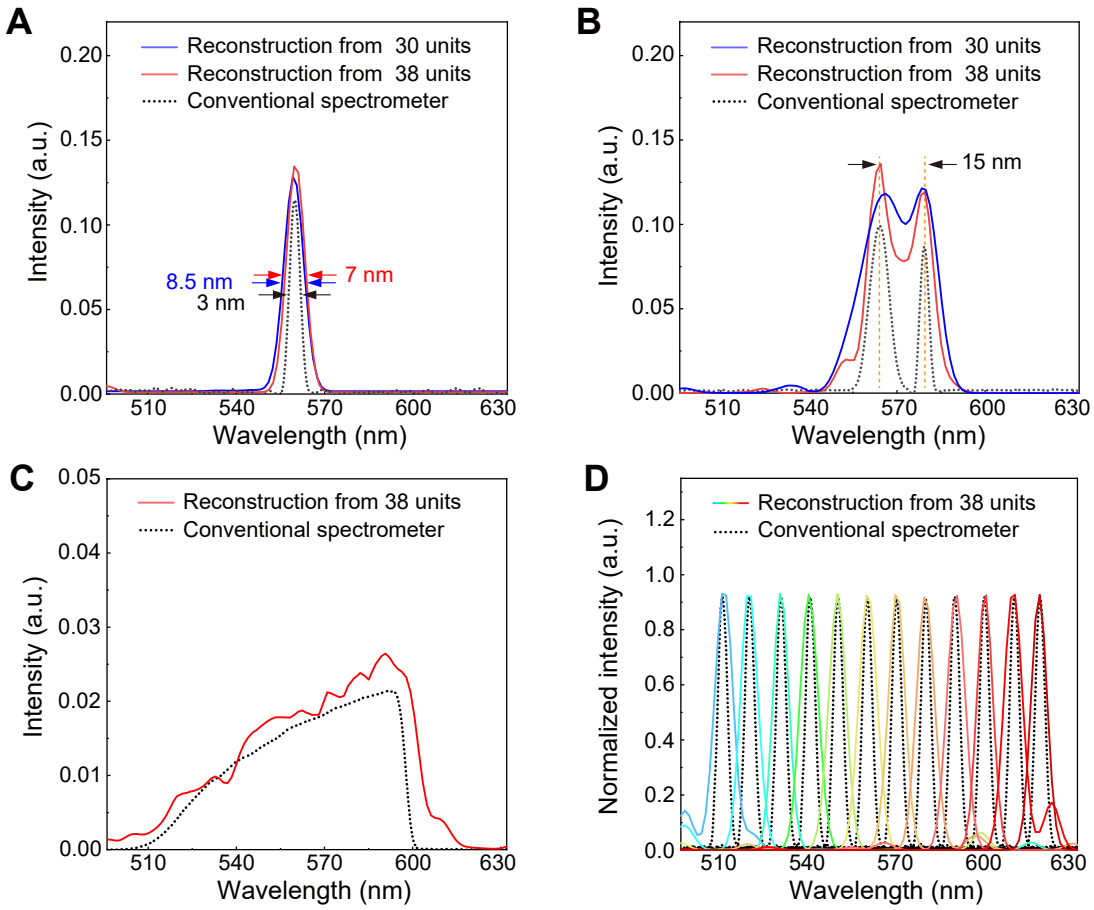

Fig. 2. Characterization of nanowire spectrometers. (A) Measurement and reconstruction of a single spectral peak at 560 nm using a 30- and 38-unit device, relative to the same signal measured by a conventional spectrometer (Thorlabs CCS100, 0.5 nm wavelength accuracy). Arrows indicate FWHM. **(B)** Two mixed narrow-band signals, with peaks separated by 15 nm, are resolved by the devices from A. **(C),(D)** Spectrum of a broadband light signal (C) and spectra of a range of monochromatic peaks across the operational wavelength span (D) as measured and reconstructed using the 38-unit device.

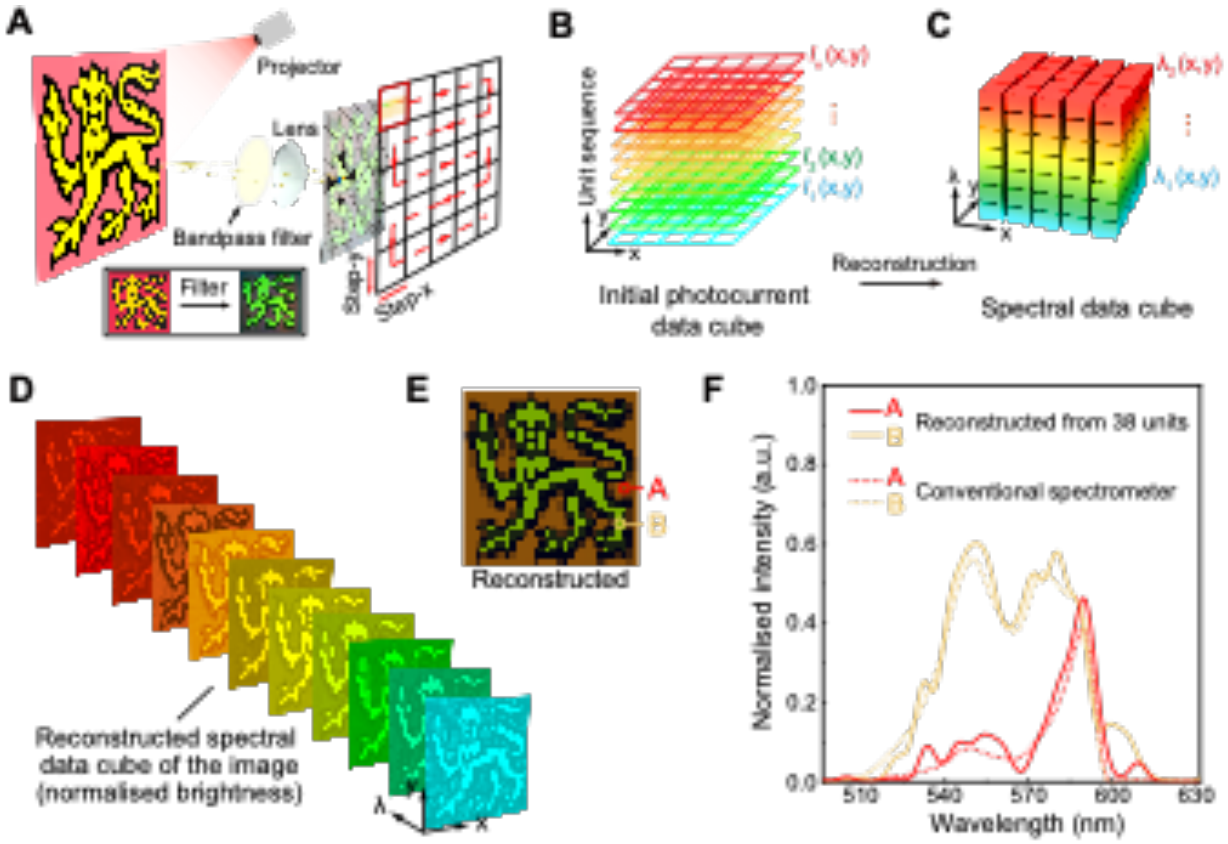

Fig. 3. Scanning spectral imaging at the macroscale. (A) Schematic of spectral imaging by our nanowire spectrometer. A bandpass filter is used to remove signals outside the detectable range of the spectrometer. Spectral imaging is conducted by scanning the nanowire spectrometer on the focal plane in a serpentine pattern. **(B)** Each pixel contains a photocurrent value from each photodetector unit, forming an initial data cube. **(C)** A spectral data cube is computationally reconstructed from the photocurrent data cube. **(D)** A series of reconstructed images at selected wavelengths. The intensity range of these images is normalized. **(E)** Pseudo-colored spectral image converted from the spectra according to CIE color matching functions. **(F)** Spectra of points A and B in (E), measured by a nanowire spectrometer and a conventional spectrometer.

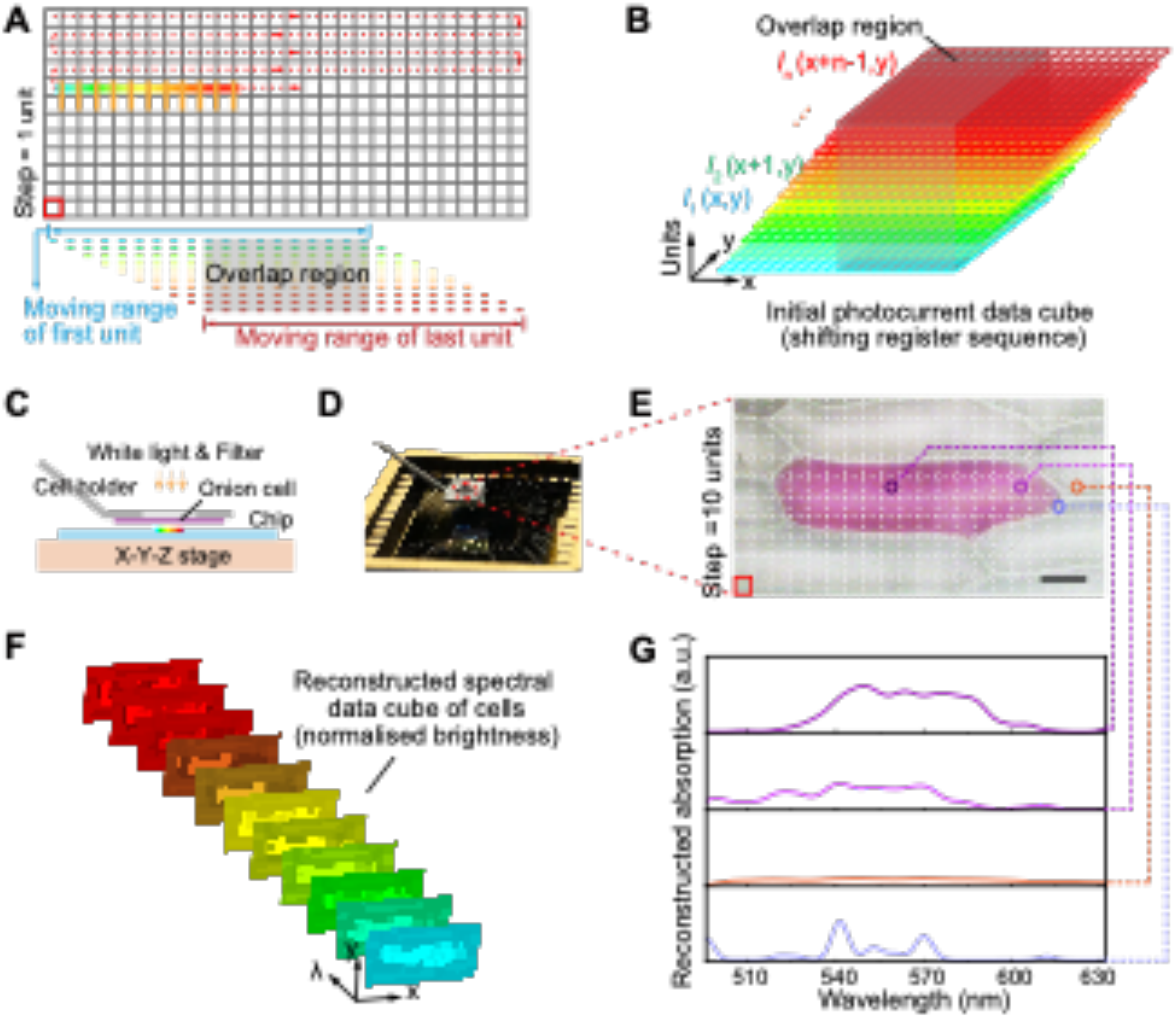

Fig. 4. Spectral imaging at the micron scale. (A) Schematic illustrating the shift register scanning strategy used when required pixel size is less than the spectrometer length. **(B)** Initial photocurrent data cube; each layer is shifted as each pixel is scanned by each unit in turn. **(C)** Schematic of the operation of cell mapping. **(D)** Photograph of the cell mapping apparatus. **(E)** Micrograph of a naturally pigmented red onion cell surrounded by transparent cells. Scale bar: 50 µm. **(F)** Absorption spectral images of the onion cell at selected wavelengths. Pixel intensity range of these images is normalized. **(G)** Reconstructed absorption spectra from different parts of the red onion cells.

References and Notes

1. N. Savage, Spectrometers. *Nat. Photonics* **3**, 601-602 (2009).
2. R. F. Wolffenbuttel, State-of-the-Art in Integrated Optical Microspectrometers. *IEEE Trans. Instrum. Meas.* **53**, 197-202 (2004).
3. O. Manzardo, H. P. Herzig, C. R. Marxer, N. F. de Rooij, Miniaturized time-scanning Fourier transform spectrometer based on silicon technology. *Opt. Lett.* **24**, 1705-1707 (1999).
4. H. Y. Zhang, X. L. Wang, J. Soos, J. Crisp, Design of a miniature solid-state NIR spectrometer. *Proc. SPIE* **2475**, 376-383 (1995).
5. D. Sander, J. Muller, Selffocussing phase transmission grating for an integrated optical microspectrometer. *Sens. Actuators A Phys.* **88**, 1-9 (2001).
6. J. Bao, M. G. Bawendi, A colloidal quantum dot spectrometer. *Nature* **523**, 67-70 (2015).
7. U. Kurokawa, B. I. Choi, C.-C. Chang, Filter-Based Miniature Spectrometers: Spectrum Reconstruction Using Adaptive Regularization. *IEEE Sens. J.* **11**, 1556-1563 (2011).
8. F. Gu, H. Yu, W. Fang, L. Tong, Broad spectral response in composition-graded CdSSe single nanowires via waveguiding excitation. *Appl. Phys. Lett.* **99**, 181111 (2011).
9. P. Ren *et al.*, Band-selective infrared photodetectors with complete-composition-range InAs(x)P(1-x) alloy nanowires. *Adv. Mater.* **26**, 7444-7449 (2014).
10. X. Hu *et al.*, Wavelength Selective Photodetectors Integrated on a Single Composition-Graded Semiconductor Nanowire. *Adv. Opt. Mater.*, 1800293 (2018).
11. C. J. Kim *et al.*, On-nanowire band-graded Si:Ge photodetectors. *Adv. Mater.* **23**, 1025-1029 (2011).
12. B. Tian, T. J. Kempa, C. M. Lieber, Single nanowire photovoltaics. *Chem. Soc. Rev.* **38**, 16-24 (2009).
13. X. Zhuang, C. Z. Ning, A. Pan, Composition and bandgap-graded semiconductor alloy nanowires. *Adv. Mater.* **24**, 13-33 (2012).
14. C.-Z. Ning, L. Dou, P. Yang, Bandgap engineering in semiconductor alloy nanomaterials with widely tunable compositions. *Nat. Rev. Mater.* **2**, 17070 (2017).
15. Z. Yang *et al.*, On-nanowire spatial band gap design for white light emission. *Nano Lett.* **11**, 5085-5089 (2011).
16. T. Kuykendall, P. Ulrich, S. Aloni, P. Yang, Complete composition tunability of InGaN nanowires using a combinatorial approach. *Nat. Mater.* **6**, 951-956 (2007).
17. F. Gu *et al.*, Spatial bandgap engineering along single alloy nanowires. *J. Am. Chem. Soc.* **133**, 2037-2039 (2011).
18. Z. Yang *et al.*, Broadly defining lasing wavelengths in single bandgap-graded semiconductor nanowires. *Nano Lett.* **14**, 3153-3159 (2014).
19. *See supplementary materials; available on Science Online.*
20. T. Yang, C. Li, Z. Wang, H. Ho, An ultra compact spectrometer based on the optical transmission through a micro interferometer array. *Optik* **124**, 1377-1385 (2013).
21. C. C. Chang, H. N. Lee, On the estimation of target spectrum for filter-array based spectrometers. *Opt. Express* **16**, 1056-1061 (2008).
22. N. Blind, E. Le Coarer, P. Kern, S. Gousset, Spectrographs for astrophotonics. *Opt. Express* **25**, 27341-27369 (2017).
23. D. J. Mulla, Twenty five years of remote sensing in precision agriculture: Key advances and remaining knowledge gaps. *Biosyst. Eng.* **114**, 358-371 (2013).

24. J. S. Bouillard, S. Vilain, W. Dickson, A. V. Zayats, Hyperspectral imaging with scanning near-field optical microscopy: applications in plasmonics. *Opt. Express* **18**, 16513-16519 (2010).
25. A. S. Stender *et al.*, Single cell optical imaging and spectroscopy. *Chem. Rev.* **113**, 2469-2527 (2013).
26. A. T. Harris, Spectral mapping tools from the earth sciences applied to spectral microscopy data. *Cytometry A* **69**, 872-879 (2006).
27. J. Pan *et al.*, Composition-tunable vertically aligned CdS(x)Se(1-x) nanowire arrays via van der Waals epitaxy: investigation of optical properties and photocatalytic behavior. *Adv. Mater.* **24**, 4151-4156 (2012).
28. A. R. Denton, N. W. Ashcroft, Vegard's law. *Phys. Rev. A* **43**, 3161-3164 (1991).
29. P. C. Hansen, *Rank-Deficient and Discrete Ill-Posed Problems*. Rank-Deficient and Discrete Ill-Posed Problems (Siam, 2005), vol. 4.
30. P. C. Hansen, Analysis of Discrete Ill-Posed Problems by Means of the L-Curve. *SIAM Review* **34**, 561-580 (1992).
31. G. H. Golub, M. Heath, G. Wahba, Generalized Cross-Validation as a Method for Choosing a Good Ridge Parameter. *Technometrics* **21**, 215-223 (1979).
32. G. Wahba, Practical Approximate Solutions to Linear Operator Equations when the Data are Noisy. *SIAM J. Numer. Anal.* **14**, 651-667 (1977).
33. P. C. Hansen, *Discrete Inverse Problems*. Discrete Inverse Problems (Siam, 2010), vol. 7.
34. J. A. Alexander-Webber *et al.*, Engineering the Photoresponse of InAs Nanowires. *ACS Appl. Mater. Interfaces* **9**, 43993-44000 (2017).
35. T. Gao, Q. H. Li, T. H. Wang, CdS nanobelts as photoconductors. *Appl. Phys. Lett.* **86**, 173105 (2005).
36. J. S. Jie *et al.*, Photoconductive characteristics of single-crystal CdS nanoribbons. *Nano Lett.* **6**, 1887-1892 (2006).
37. H. Kind, H. Yan, B. Messer, M. Law, P. Yang, Nanowire Ultraviolet Photodetectors and Optical Switches. *Adv. Mater.* **14**, 158-160 (2002).
38. K. M. Bryan *et al.*, Inexpensive photonic crystal spectrometer for colorimetric sensing applications. *Optics express* **21**, 4411-4423 (2013).
39. C. C. Chang, N. T. Lin, U. Kurokawa, B. Il Choi, Spectrum reconstruction for filter-array spectrum sensor from sparse template selection. *Optical Engineering* **50**, 114402 (2011).
40. J. Oliver, W. Lee, S. Park, H. N. Lee, Improving resolution of miniature spectrometers by exploiting sparse nature of signals. *Optics express* **20**, 2613-2625 (2012).
41. S. Zhang, Y. Dong, H. Fu, S. L. Huang, L. Zhang, A Spectral Reconstruction Algorithm of Miniature Spectrometer Based on Sparse Optimization and Dictionary Learning. *Sensors* **18**, (2018).
42. G. Lu, B. Fei, Medical hyperspectral imaging: a review. *J Biomed Opt* **19**, 10901 (2014).
43. P. J. Lapray, X. Wang, J. B. Thomas, P. Gouton, Multispectral filter arrays: recent advances and practical implementation. *Sensors (Basel)* **14**, 21626-21659 (2014).
44. B. Geelen, N. Tack, A. Lambrechts, A compact snapshot multispectral imager with a monolithically integrated per-pixel filter mosaic. **8974**, 89740L (2014).
45. N. Hagen, M. W. Kudenov, Review of snapshot spectral imaging technologies. *Optical Engineering* **52**, (2013).
46. Z. Wang *et al.*, Single-shot on-chip spectral sensors based on photonic crystal slabs. *Nature communications* **10**, 1020 (2019).

47. A. Tittl *et al.*, Imaging-based molecular barcoding with pixelated dielectric metasurfaces. *Science* **360**, 1105-1109 (2018).
48. F. Yesilkoy *et al.*, Ultrasensitive hyperspectral imaging and biodetection enabled by dielectric metasurfaces. *Nature Photonics* **13**, 390-396 (2019).
49. B. Cerjan, N. J. Halas, Toward a Nanophotonic Nose: A Compressive Sensing-Enhanced, Optoelectronic Mid-Infrared Spectrometer. *ACS Photonics* **6**, 79-86 (2018).
50. M. Faraji-Dana *et al.*, Compact folded metasurface spectrometer. *Nature communications* **9**, 4196 (2018).
51. Y. Z. Long, M. Yu, B. Sun, C. Z. Gu, Z. Fan, Recent advances in large-scale assembly of semiconducting inorganic nanowires and nanofibers for electronics, sensors and photovoltaics. *Chemical Society reviews* **41**, 4560-4580 (2012).
52. D. Tsivion, M. Schvartzman, R. Popovitz-Biro, P. von Huth, E. Joselevich, Guided growth of millimeter-long horizontal nanowires with controlled orientations. *Science* **333**, 1003-1007 (2011).
53. D. M. Kita *et al.*, High-performance and scalable on-chip digital Fourier transform spectroscopy. *Nature communications* **9**, 4405 (2018).
54. G. Calafiore *et al.*, Holographic planar lightwave circuit for on-chip spectroscopy. *Light: Science & Applications* **3**, e203 (2014).
55. *Hamamatsu mini-spectrometer micro series C12666MA*. (https://www.hamamatsu.com/eu/en/product/type/C12666MA/index.html).

Acknowledgments: We thank Yu Ye, Henri Jussila, Ayaz Ali, Shuo Gao, Xiaolong Chen, Guohua Hu, Yubo Wang, George Gordon, Jiangen Pan, Jianbin Liu, Bigeng Chen, Sarwat Baig and Hannah Joyce for discussion. Girish Rughoobur and Xingyi Wu for use of probe station.

Funding: Z. Y. acknowledges support from Cambridge Trust, T. A. O. from EPSRC (EP/L016087/1), J. A. W. from the Royal Commission for the Exhibition of 1851, C. W. for the CRUK Pioneer Award (C55962/A24669), A. Z. from EPSRC (EP/M013812/1), Z. S. from Business Finland (A-Photonics), Academy of Finland, the ERC (834742), the EU Horizon 2020 (820423), and Q. Y. and T. H. from the Royal Society.

Author contributions: Z. Y. and T. A. O. contributed equally to this work. Z. Y. conceived the spectrometer concept, performed experiments, analyzed data and prepared figures. T. A. O. fabricated and characterized devices, and analyzed data. H. C., M. O. developed the MATLAB program. T. H. supervised the project and advised on device optimization. F. G., J. A. W., C. W., P. W., A. Z., and W. C. provided measurement support. X. W., S. H., Y. W., M. Z., T. C. W., L. D., Z. S., Q. Y., L. T. contributed to the interpretation of the data. Z. Y., T. A. O., Z. S. and T. H. wrote the manuscript, with contributions from all other co-authors.

Competing interests: The invention described in this report was the subject of a patent filing in August 2019 (inventors: Z. Y., T. A. O. and T. H.).

Data and materials availability: All data needed to evaluate the conclusions in the paper are present in the main text or the supplementary materials.

Supplementary Materials:

Materials and Methods

Supplementary Text

Figures S1-S18

Table S1

References (*27*-*55*)

5